

Double-heavy tetraquarks

Gang Yang^{1,*}, Jialun Ping^{2,†} and Jorge Segovia^{3,‡}

¹*Department of Physics and State Key Laboratory of Low-Dimensional Quantum Physics, Tsinghua University, Beijing 100084, People's Republic of China*

²*Department of Physics and Jiangsu Key Laboratory for Numerical Simulation of Large Scale Complex Systems, Nanjing Normal University, Nanjing 210023, People's Republic of China*

³*Departamento de Sistemas Físicos, Químicos y Naturales, Universidad Pablo de Olavide, E-41013 Sevilla, Spain*



(Received 10 November 2019; published 2 January 2020)

In the framework of the chiral quark model along with complex scaling range, we perform a dynamical study on the low-lying S -wave double-heavy tetraquark states ($QQ\bar{q}\bar{q}$, $Q = c, b$ and $q = u, d$) with an accurate computing approach, Gaussian expansion method. The meson-meson and diquark-antidiquark configurations within all possible color structures for spin-parity quantum numbers $J^P = 0^+, 1^+$, and 2^+ and in the 0 and 1 isospin sectors are considered. Possible tightly bound and narrow resonance states are obtained for double-charm and double-bottom tetraquarks with $IJ^P = 01^+$, and these exotic states are also obtained in charm-bottom tetraquarks with 00^+ and 01^+ quantum numbers. Only a loosely bound state is found in charm-bottom tetraquarks of 02^+ states. All of these bound states within meson-meson configurations are loosely bound whether in color-singlet channels or coupling to hidden-color ones. However, compact structures are available in diquark-antidiquark channels except for charm-bottom tetraquarks in 02^+ states.

DOI: [10.1103/PhysRevD.101.014001](https://doi.org/10.1103/PhysRevD.101.014001)

I. INTRODUCTION

The story of exotic hadronic states can be dated back to the announcement of $X(3872)$ in the invariant mass spectrum of $J/\psi\pi^+\pi^-$ produced in $B^\pm \rightarrow K^\pm X(3872) \rightarrow K^\pm J/\psi\pi^+\pi^-$ decays by the Belle Collaboration in 2003 [1]. This charmoniumlike state was confirmed by other experimental collaborations [2–4] during the following years. However, theoretical explanations on $X(3872)$ are still controversial: (i) In spite of the predicted mass of $\chi_{c1}(2P)$ being too high (~ 3.95 GeV) to be identified with $X(3872)$ [5–8], the radiative decays are better described in charmonium structure [9,10], (ii) mass near the $D^0\bar{D}^{*0}$ threshold is compatible with the molecular state [11–14] and the comprehensible isospin-breaking decay process of $X(3872) \rightarrow J/\psi\rho$, (iii) the $X(3872)$ is also described as a compact diquark-antidiquark state [15], and (iv) the existence of $c\bar{c}$ bound states dressed by a DD^* molecular

component is proposed [16–20]. In fact, during the past 16 years, more than two dozen unconventional charmonium- and bottomoniumlike states, the so-called XYZ mesons, have been observed at B factories (*BABAR*, Belle and CLEO), τ -charm facilities (CLEO-c and BESIII), and also proton-(anti)proton colliders (CDF, D0, LHCb, ATLAS, and CMS), e.g., $Y(4260)$ discovered by the *BABAR* Collaboration in 2005 [21], $Z^+(4430)$ discovered by the Belle Collaboration in 2007 [22], $Y(4140)$ discovered by the CDF Collaboration in 2009 [23], and $Z_c^+(3900)$ discovered by the BESIII Collaboration in 2013 [24], etc. Meanwhile, remarkable achievements in the baryon sectors are also valuable. In 2015, two exotic hidden-charmonium pentaquarks, $P_c^+(4380)$ and $P_c^+(4450)$, were announced by the LHCb Collaboration [25] in the Λ_b^0 decay $\Lambda_b^0 \rightarrow J/\psi K^- p$, and in 2019, with higher statistical significance, one new pentaquark state $P_c^+(4312)$ was found by the same collaboration, and the previously reported wide state $P_c^+(4450)$ was superseded by two narrow ones, $P_c^+(4440)$ and $P_c^+(4457)$ [26]. A review on these exotic states can be found in Refs. [27–30].

Apparently, these facts have triggered a large number of theoretical investigations on the new hadronic zoo where the conventional configuration of mesons and baryons as, respectively, quark-antiquark and three-quark bound states is being left behind. In the fully heavy tetraquarks sector, the CMS Collaboration claimed an observation of pair

*ygz0788a@sina.com

†jlping@njnu.edu.cn

‡jsegovia@upo.es

Published by the American Physical Society under the terms of the [Creative Commons Attribution 4.0 International license](https://creativecommons.org/licenses/by/4.0/). Further distribution of this work must maintain attribution to the author(s) and the published article's title, journal citation, and DOI. Funded by SCOAP³.

production of $\Upsilon(1S)$ mesons at the LHC in pp collisions [31], and this may indicate a $bb\bar{b}\bar{b}$ tetraquark state with a mass of 18.4 GeV. A significant peak at ~ 18.2 GeV was observed in Cu +Au collisions at the Relativistic Heavy Ion Collider [32]. However, no evidence has been provided from the LHCb Collaboration by searching for the $\Upsilon(1S)\mu^+\mu^-$ invariant mass spectrum [33]. Extensive theoretical works with different schemes are devoted to these extremely nonrelativistic systems, $QQ\bar{Q}\bar{Q}$ ($Q = c, b$): The existence of $bb\bar{b}\bar{b}$ bound state is supported by a phenomenological model calculation [34–37], QCD sum rules [38,39], and the diffusion Monte Carlo method [40]. A narrow $cc\bar{c}\bar{c}$ tetraquark state in the mass region 5–6 GeV has been predicted by the Bethe-Salpeter approach [41] and also in several phenomenological models [34,42–44]. However, there are still intense debates on the observation of these exotic states. No $cc\bar{c}\bar{c}$ and $bb\bar{b}\bar{b}$ bound states can be formed within effective model calculations [45–50] and lattice QCD [51], but possible stable or narrow states in the $bb\bar{b}\bar{c}$ and $bc\bar{b}\bar{c}$ systems [45,46].

Nevertheless, results on double-heavy tetraquark states investigated by different kinds of theoretical approaches are more compatible. In the heavy quark limit, a stable and extremely narrow $bb\bar{u}\bar{d}$ tetraquark state with the $J^P = 1^+$ must exist [52]. In Ref. [53], the predicted mass of the $bb\bar{u}\bar{d}$ state within the same spin parity is 10389 ± 12 MeV. The mass, lifetime, and decay modes of this tetraquark are investigated in Ref. [54]. A compact double-bottom tetraquark state with $IJ^P = 01^+$ is also presented in heavy-ion collisions at the LHC [55], and actually, in 1988, the dimeson $T(bb\bar{u}\bar{d})$ had already been proposed [56]. Besides, a narrow $(bb)(\bar{u}\bar{d})$ diquark-antidiquark state with $IJ^P = 01^+$ is predicted in Ref. [57]. A $\bar{b}\bar{b}ud$ bound state also with $IJ^P = 01^+$ is stable against the strong and electromagnetic decay, and its mass is $10476 \pm 24 \pm 10$ MeV by lattice QCD [58]; this deeply bound state is supported also by the same formalism in Refs. [59,60]. Meanwhile, there are also QCD sum rules predicting a mass 7105 ± 155 MeV for a $bc\bar{u}\bar{d}$ axial-vector tetraquark state [61], and a $I(J^P) = 0(1^+) ud\bar{c}\bar{d}$ tetraquark which binding energy is 15–61 MeV with respect to the $\bar{D}B^*$ threshold is proposed by Ref. [62]. Moreover, the production potential of double-heavy tetraquarks at a Tera-Z factory and the LHC are estimated by a Monte Carlo simulation [63,64]. However, no strong indication for any bound state or narrow resonance of tetraquarks in the charm sector are found in a lattice study [65]. Some other types of tetraquark states along with decay properties are explored in Refs. [66–68].

We study herein, within a complex scaling range of the chiral quark model formalism, the possibility of having tetraquark bound and resonance states in the double-heavy sector with quantum numbers $J^P = 0^+, 1^+$, and 2^+ and in the 0 and 1 isospin sectors. Two configurations, meson-meson and diquark-antidiquark structures, are considered.

In particular, color-singlet and hidden-color channels for the dimeson configuration and color triplet-antitriplet and sextet-antisextet channels for the diquark-antidiquark one along with their couplings are all employed for each quantum state. The bound states, if possible, their internal structures, and components in the complete coupled-channel calculation are analyzed by computing the distances among any pair of quarks and the contributions of each channel's wave functions. Meanwhile, masses and widths for possible resonance states are also studied in the complete coupled channels.

The four-body bound state problem is implemented by two strong foundations: the Gaussian expansion method (GEM) [69], which has been demonstrated to be as accurate as a Faddeev calculation (see, for instance, Figs. 15 and 16 in Ref. [69]), and the chiral quark model, which has been successfully applied to hadron [8,70–75], hadron-hadron [76–80], and multi-quark [81–84] phenomenology. However, due to the complexity of the coupled-channel case for scattering and resonance states, it is difficult to solve a scattering issue together with a resonance one. In this work, a powerful technique, the complex scaling method (CSM), is employed, and this is also the first time for its application to tetraquark states in hadronic physics. During the past decades, it has been extensively applied to nuclear physics problems [85,86] and recently also in the study of charmed dibaryon resonances [87]. The CSM is quite different from a real range one, for the scattering, resonance, and bound states can all be concordant in one calculation (see Fig. 1, a schematic distribution of the complex energy of two-body by the CSM according to Ref. [86]); namely, the scattering states can be solved as a bound states problem without a Lippmann-Schwinger equation or some scattering issues related, and the resonance pole will be fixed in the complex plane. A brief

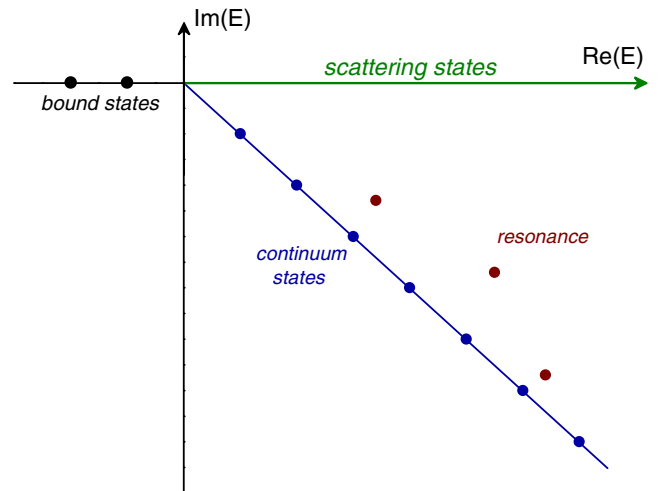


FIG. 1. Schematic complex energy distribution in the single-channel two-body system.

sketch for the application of the CSM in tetraquark states will be shown in the next section.

The structure of this paper is organized in the following way. In Sec. II, the theoretical framework which includes the chiral quark model, tetraquark wave functions, GEM, and CSM is briefly presented and discussed. Section III is devoted to the analysis and discussion on the obtained results. The summary and some prospects are presented in Sec. IV.

II. THEORETICAL FRAMEWORK

With half a century development in high-energy physics, the QCD-inspired quark models are still the main tool to shed some light on the nature of the multi-quark candidates observed by experimentalists. Particularly, the chiral quark model has witnessed great achievements in our early work on possible hidden-charm pentaquark bound states with quantum numbers $IJ^P = \frac{1}{2}(\frac{1}{2})^\pm, \frac{1}{2}(\frac{3}{2})^\pm, \text{ and } \frac{1}{2}(\frac{5}{2})^\pm$ [82]. Therein, the properties were compared with those associated with the hidden-charm pentaquark signals observed by the LHCb Collaboration in 2015 [25]. Although three new hidden-charm pentaquarks were also reported by the same collaboration in 2019 [26], these states are not discussed exactly in the present work. Herein, the application of the chiral quark model in double-heavy tetraquark states is quite expected.

The general form of our four-body Hamiltonian in the complex scaling method is

$$H(\theta) = \sum_{i=1}^4 \left(m_i + \frac{\vec{p}_i^2}{2m_i} \right) - T_{\text{CM}} + \sum_{j>i=1}^4 V(\vec{r}_{ij}e^{i\theta}), \quad (1)$$

where the center-of-mass kinetic energy T_{CM} is subtracted without losing generality, since we mainly focus on the internal relative motions of the multi-quark system. The interaction part is of two-body potential

$$V(\vec{r}_{ij}e^{i\theta}) = V_{\text{CON}}(\vec{r}_{ij}e^{i\theta}) + V_{\text{OGE}}(\vec{r}_{ij}e^{i\theta}) + V_{\chi}(\vec{r}_{ij}e^{i\theta}) \quad (2)$$

and includes the color-confining, one-gluon exchange and Goldstone-boson exchange interactions. Note herein that only the central and spin of potential are considered; since our main goal of the present work is to perform a systematical study on the low-lying S -wave double-heavy tetraquark states, it is reasonable for the absence of spin-orbit and tensor contributions. One can see that the coordinates of relative motions between quarks are transformed with a complex rotation $\vec{r} \rightarrow \vec{r}e^{i\theta}$. Accordingly, in the framework of a complex range, the four-body systems are solved in a complex scaled Schrödinger equation:

$$[H(\theta) - E(\theta)]\Psi_{JM}(\theta) = 0. \quad (3)$$

According to the ABC theorem [88,89], there are three types of complex eigenenergies of Eq. (3) as shown in Fig. 1:

- (i) The bound state below the threshold is always located on the negative axis of real energy.
- (ii) The discretized continuum states are aligned along the cut line with a rotated angle of 2θ related to the real axis.
- (iii) The resonance state is a fixed pole under the complex scaling transformation and is located above the continuum cut line. The resonance width is given by $\Gamma = -2\text{Im}(E)$.

As an illustration to each interaction potential in Eq. (2), first, color confinement should be encoded in the non-Abelian character of QCD. It has been demonstrated by lattice QCD that multigluon exchanges produce an attractive linearly rising potential proportional to the distance between infinite-heavy quarks [90]. However, the spontaneous creation of light-quark pairs from the QCD vacuum may give rise at the same scale to a breakup of the created color flux tube [90]. These two phenomenological observations are mimicked by the following expression when $\theta = 0^\circ$:

$$V_{\text{CON}}(\vec{r}_{ij}e^{i\theta}) = [-a_c(1 - e^{-\mu_c r_{ij}e^{i\theta}}) + \Delta](\vec{\lambda}_i^c \cdot \vec{\lambda}_j^c), \quad (4)$$

where a_c , μ_c , and Δ are model parameters and the SU(3) color Gell-Mann matrices are denoted as λ^c . One can see in Eq. (4) that the potential is linear at short interquark distances with an effective confinement strength $\sigma = -a_c\mu_c(\vec{\lambda}_i^c \cdot \vec{\lambda}_j^c)$, while V_{CON} becomes constant ($\Delta - a_c$) $(\vec{\lambda}_i^c \cdot \vec{\lambda}_j^c)$ at large distances.

The one-gluon exchange potential which includes the Coulomb and color-magnetism interactions is given by

$$V_{\text{OGE}}(\vec{r}_{ij}e^{i\theta}) = \frac{1}{4}\alpha_s(\vec{\lambda}_i^c \cdot \vec{\lambda}_j^c) \left[\frac{1}{r_{ij}e^{i\theta}} - \frac{1}{6m_i m_j} (\vec{\sigma}_i \cdot \vec{\sigma}_j) \frac{e^{-r_{ij}e^{i\theta}/r_0(\mu)}}{r_{ij}e^{i\theta} r_0^2(\mu)} \right], \quad (5)$$

where m_i and $\vec{\sigma}$ are the quark mass and the Pauli matrices, respectively. The contact term of the central potential in complex range has been regularized as

$$\delta(\vec{r}_{ij}e^{i\theta}) \sim \frac{1}{4\pi r_0^2} \frac{e^{-r_{ij}e^{i\theta}/r_0}}{r_{ij}e^{i\theta}}, \quad (6)$$

with $r_0(\mu_{ij}) = \hat{r}_0/\mu_{ij}$ a regulator that depends on μ_{ij} , the reduced mass of the quark-(anti)quark pair.

The QCD strong coupling constant α_s (an effective scale-dependent strong coupling constant) offers a consistent description of mesons and baryons from light to heavy quark sectors in a wide energy range, and we use the frozen coupling constant of, for instance, Ref. [7]:

$$\alpha_s(\mu_{ij}) = \frac{\alpha_0}{\ln\left(\frac{\mu_{ij}^2 + \mu_0^2}{\Lambda_0^2}\right)}, \quad (7)$$

in which α_0 , μ_0 , and Λ_0 are parameters of the model.

The central terms of Goldstone-boson exchange interaction in the CSM can be written as

$$V_\pi(\vec{r}_{ij}e^{i\theta}) = \frac{g_{ch}^2}{4\pi} \frac{m_\pi^2}{12m_i m_j} \frac{\Lambda_\pi^2}{\Lambda_\pi^2 - m_\pi^2} m_\pi \left[Y(m_\pi r_{ij} e^{i\theta}) - \frac{\Lambda_\pi^3}{m_\pi^3} Y(\Lambda_\pi r_{ij} e^{i\theta}) \right] (\vec{\sigma}_i \cdot \vec{\sigma}_j) \sum_{a=1}^3 (\lambda_i^a \cdot \lambda_j^a), \quad (8)$$

$$V_\sigma(\vec{r}_{ij}e^{i\theta}) = -\frac{g_{ch}^2}{4\pi} \frac{\Lambda_\sigma^2}{\Lambda_\sigma^2 - m_\sigma^2} m_\sigma \left[Y(m_\sigma r_{ij} e^{i\theta}) - \frac{\Lambda_\sigma}{m_\sigma} Y(\Lambda_\sigma r_{ij} e^{i\theta}) \right], \quad (9)$$

$$V_K(\vec{r}_{ij}e^{i\theta}) = \frac{g_{ch}^2}{4\pi} \frac{m_K^2}{12m_i m_j} \frac{\Lambda_K^2}{\Lambda_K^2 - m_K^2} m_K \left[Y(m_K r_{ij} e^{i\theta}) - \frac{\Lambda_K^3}{m_K^3} Y(\Lambda_K r_{ij} e^{i\theta}) \right] (\vec{\sigma}_i \cdot \vec{\sigma}_j) \sum_{a=4}^7 (\lambda_i^a \cdot \lambda_j^a), \quad (10)$$

$$V_\eta(\vec{r}_{ij}e^{i\theta}) = \frac{g_{ch}^2}{4\pi} \frac{m_\eta^2}{12m_i m_j} \frac{\Lambda_\eta^2}{\Lambda_\eta^2 - m_\eta^2} m_\eta \left[Y(m_\eta r_{ij} e^{i\theta}) - \frac{\Lambda_\eta^3}{m_\eta^3} Y(\Lambda_\eta r_{ij} e^{i\theta}) \right] (\vec{\sigma}_i \cdot \vec{\sigma}_j) [\cos \theta_p (\lambda_i^8 \cdot \lambda_j^8) - \sin \theta_p], \quad (11)$$

where $Y(x) = e^{-x}/x$ is the standard Yukawa function. The physical η meson is considered by introducing the angle θ_p instead of the octet one. The λ^a are the SU(3) flavor Gell-Mann matrices. Taken from their experimental values, m_π , m_K , and m_η are the masses of the SU(3) Goldstone bosons. The value of m_σ is determined through the partially conserved axial-vector current relation $m_\sigma^2 \simeq m_\pi^2 + 4m_{u,d}^2$ [91]. Finally, the chiral coupling constant g_{ch} is determined from the πNN coupling constant through

$$\frac{g_{ch}^2}{4\pi} = \frac{9}{25} \frac{g_{\pi NN}^2}{4\pi} \frac{m_{u,d}^2}{m_N^2}, \quad (12)$$

which assumes that flavor SU(3) is an exact symmetry broken only by the different mass of the strange quark.

One needs to mention that the chiral quark-(anti)quark interaction plays a role only between two light quarks, and it is invalid for the other heavy-light and heavy-heavy quark pairs due to the isospin symmetry breaking. The model parameters which are listed in Table I have been fixed in

TABLE I. Model parameters.

Quark masses	$m_u = m_d$ (MeV)	313
	m_c (MeV)	1752
	m_b (MeV)	5100
Goldstone bosons	$\Lambda_\pi = \Lambda_\sigma$ (fm ⁻¹)	4.20
	Λ_η (fm ⁻¹)	5.20
	$g_{ch}^2/(4\pi)$	0.54
	θ_p (°)	-15
Confinement	a_c (MeV)	430
	μ_c (fm ⁻¹)	0.70
	Δ (MeV)	181.10
	α_0	2.118
	Λ_0 (fm ⁻¹)	0.113
OGE	$\hat{\mu}_0$ (MeV)	36.976
	\hat{r}_0 (MeV fm)	28.170

advance reproducing hadron [8,70–74], hadron-hadron [76–80], and multi-quark [81–84] phenomenology.

Four fundamental degrees of freedom in quark level—color, flavor, spin, and space—are generally accepted in the QCD theory, and the multi-quark system wave function is a product of these four terms. In Fig. 2, we show two kinds of configurations for double-heavy tetraquarks $QQ\bar{q}\bar{q}$ ($q = u, d$ and $Q = c, b$). In particular, Fig. 2(a) is the meson-meson structure, and the diquark-antidiquark one is of Fig. 2(b); both of them and their coupling are considered in our investigation.

In fact, one structure is enough for the calculation, if all excitation states are taken into account. However, it is clearly too difficult to use this approach. An economic way is to combine different structures which are all kept in the ground state to do the calculation. Moreover, the effect of identical particle exchange in these two configurations will lead to a singular matrix when diagonalizing the Hamiltonian. To solve the double counting problem, the eigenfunction method is employed. First, the overlap matrix is diagonalized, and the eigenvectors with eigenvalue 0 are abandoned, then, we reconstruct the Hamiltonian matrix by using the remained eigenvectors, and last, the new Hamiltonian matrix is diagonalized to obtain the energies of the system.

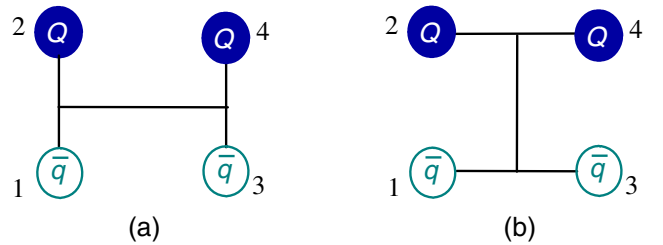


FIG. 2. Two types of configurations in double-heavy tetraquarks. (a) is the meson-meson structure, and (b) is the diquark-antidiquark one ($Q = c, b$ and $q = u, d$).

Concerning the color degree of freedom, more richer structures in the multiquark system will be discussed than conventional hadrons ($q\bar{q}$ mesons and qqq baryons). The colorless wave function of four-quark systems in the dimeson configuration can be obtained by either a color-singlet or a hidden-color channel or both. However, this is not a unique path, for the authors of Refs. [92,93] assert that it is enough to consider the color-singlet channel when all possible excited states of a system are included. After a comparison, a more economical way of computing through considering all the possible color structures and their coupling is employed. First, in the color SU(3) group, the wave functions of the color-singlet (two color-singlet clusters coupling, 1×1) and hidden-color (two color-octet clusters coupling, 8×8) channel in the dimeson configuration in Fig. 2(a) is signed as χ_1^c and χ_2^c , respectively,

$$\chi_1^c = \frac{1}{3}(\bar{r}r + \bar{g}g + \bar{b}b) \times (\bar{r}r + \bar{g}g + \bar{b}b), \quad (13)$$

$$\begin{aligned} \chi_2^c = & \frac{\sqrt{2}}{12}(3\bar{b}r\bar{r}b + 3\bar{g}r\bar{r}g + 3\bar{b}g\bar{g}b + 3\bar{g}b\bar{b}g + 3\bar{r}g\bar{g}r \\ & + 3\bar{r}b\bar{b}r + 2\bar{r}r\bar{r}r + 2\bar{g}g\bar{g}g + 2\bar{b}b\bar{b}b - \bar{r}r\bar{g}g \\ & - \bar{g}g\bar{r}r - \bar{b}b\bar{g}g - \bar{b}b\bar{r}r - \bar{g}g\bar{b}b - \bar{r}r\bar{b}b). \end{aligned} \quad (14)$$

In addition, also according to an increased sequence of numbers labeled in Fig. 2, the color wave functions of the diquark-antidiquark structure shown in Fig. 2(b) are χ_3^c (color triplet-antitriplet clusters coupling, $3 \times \bar{3}$) and χ_4^c (color sextet-antisextet clusters coupling, $6 \times \bar{6}$), respectively:

$$\begin{aligned} \chi_3^c = & \frac{\sqrt{3}}{6}(\bar{r}r\bar{g}g - \bar{g}r\bar{r}g + \bar{g}g\bar{r}r - \bar{r}g\bar{g}r + \bar{r}r\bar{b}b \\ & - \bar{b}r\bar{r}b + \bar{b}b\bar{r}r - \bar{r}b\bar{b}r + \bar{g}g\bar{b}b - \bar{b}g\bar{g}b \\ & + \bar{b}b\bar{g}g - \bar{g}b\bar{b}g), \end{aligned} \quad (15)$$

$$\begin{aligned} \chi_4^c = & \frac{\sqrt{6}}{12}(2\bar{r}r\bar{r}r + 2\bar{g}g\bar{g}g + 2\bar{b}b\bar{b}b + \bar{r}r\bar{g}g + \bar{g}r\bar{r}g \\ & + \bar{g}g\bar{r}r + \bar{r}g\bar{g}r + \bar{r}r\bar{b}b + \bar{b}r\bar{r}b + \bar{b}b\bar{r}r \\ & + \bar{r}b\bar{b}r + \bar{g}g\bar{b}b + \bar{b}g\bar{g}b + \bar{b}b\bar{g}g + \bar{g}b\bar{b}g). \end{aligned} \quad (16)$$

As for the flavor degree of freedom, due to the quark contents of the presently investigated four-quark systems being two heavy quarks ($Q = c, d$) and two light anti-quarks ($\bar{q} = \bar{u}, \bar{d}$), only isospin $I = 0$ and 1 will be obtained. Moreover, the flavor wave functions signed as χ_{1,M_I}^{fi} with the superscript $i = 1, 2$, and 3 are of $cc\bar{q}\bar{q}$, $bb\bar{q}\bar{q}$, and $cb\bar{q}\bar{q}$ systems, respectively. The specific wave functions read as follows:

$$\chi_{0,0}^{f1} = \sqrt{\frac{1}{2}}(\bar{u}c\bar{d}c - \bar{d}c\bar{u}c), \quad (17)$$

$$\chi_{1,-1}^{f1} = \bar{u}c\bar{u}c, \quad (18)$$

$$\chi_{0,0}^{f2} = \sqrt{\frac{1}{2}}(\bar{u}b\bar{d}b - \bar{d}b\bar{u}b), \quad (19)$$

$$\chi_{1,-1}^{f2} = \bar{u}b\bar{u}b, \quad (20)$$

$$\chi_{0,0}^{f3} = \sqrt{\frac{1}{2}}(\bar{u}c\bar{d}b - \bar{d}c\bar{u}b), \quad (21)$$

$$\chi_{1,-1}^{f3} = \bar{u}c\bar{u}b, \quad (22)$$

where the third component of the isospin M_I is set to be equal to the absolute value of total one I without loss of generality, for there is no interplay in the Hamiltonian that can distinguish such a component.

We consider herein four-quark bound states with total spin S ranging from 0 to 2. Since there is not any spin-orbital coupling-dependent potential included in our Hamiltonian, the third component (M_S) of tetraquark spin can be assumed to be equal to the total one without the loss of generality, too. Our total spin wave functions χ_{S,M_S}^σ are given by

$$\chi_{0,0}^{\sigma 1}(4) = \chi_{00}^\sigma \chi_{00}^\sigma, \quad (23)$$

$$\chi_{0,0}^{\sigma 2}(4) = \frac{1}{\sqrt{3}}(\chi_{11}^\sigma \chi_{1,-1}^\sigma - \chi_{10}^\sigma \chi_{10}^\sigma + \chi_{1,-1}^\sigma \chi_{11}^\sigma), \quad (24)$$

$$\chi_{1,1}^{\sigma 1}(4) = \chi_{00}^\sigma \chi_{11}^\sigma, \quad (25)$$

$$\chi_{1,1}^{\sigma 2}(4) = \chi_{11}^\sigma \chi_{00}^\sigma, \quad (26)$$

$$\chi_{1,1}^{\sigma 3}(4) = \frac{1}{\sqrt{2}}(\chi_{11}^\sigma \chi_{10}^\sigma - \chi_{10}^\sigma \chi_{11}^\sigma), \quad (27)$$

$$\chi_{2,2}^{\sigma 1}(4) = \chi_{11}^\sigma \chi_{11}^\sigma. \quad (28)$$

These expressions are obtained by considering the coupling of two subcluster spin wave functions with SU(2) algebra, and the necessary bases are read as

$$\chi_{11}^\sigma = \alpha\alpha, \quad \chi_{1,-1}^\sigma = \beta\beta, \quad (29)$$

$$\chi_{10}^\sigma = \frac{1}{\sqrt{2}}(\alpha\beta + \beta\alpha), \quad (30)$$

$$\chi_{00}^\sigma = \frac{1}{\sqrt{2}}(\alpha\beta - \beta\alpha). \quad (31)$$

Here, one important thing needs to be mentioned that the spin wave functions of Eq. (25) and (26) are equivalent for

two D - or B -meson configurations of the tetraquark state. Namely, the calculated masses of DD^* and D^*D are exactly the same (also for BB^*), and obviously, this is a trivial fact in the hadron level.

Among the different methods to solve the Schrödinger-like four-body bound state equation, we use the Rayleigh-Ritz variational principle, which is one of the most extended tools to solve eigenvalue problems due to its simplicity and flexibility. Meanwhile, the choice of basis to expand the intrinsic wave function of state is of great importance. In the relative motion coordinates of four-quark systems, the spatial wave function is written as follows:

$$\psi_{LM_L}(\theta) = [[\phi_{n_1 l_1}(\vec{\rho} e^{i\theta}) \phi_{n_2 l_2}(\vec{\lambda} e^{i\theta})]_l \phi_{n_3 l_3}(\vec{R} e^{i\theta})]_{LM_L}, \quad (32)$$

where the internal Jacobi coordinates for Fig. 2(a) of the meson-meson configuration are defined as

$$\vec{\rho} = \vec{x}_1 - \vec{x}_2, \quad (33)$$

$$\vec{\lambda} = \vec{x}_3 - \vec{x}_4, \quad (34)$$

$$\vec{R} = \frac{m_1 \vec{x}_1 + m_2 \vec{x}_2}{m_1 + m_2} - \frac{m_3 \vec{x}_3 + m_4 \vec{x}_4}{m_3 + m_4}, \quad (35)$$

and the diquark-antidiquark structure of Fig. 2(b) are

$$\vec{\rho} = \vec{x}_1 - \vec{x}_3, \quad (36)$$

$$\vec{\lambda} = \vec{x}_2 - \vec{x}_4, \quad (37)$$

$$\vec{R} = \frac{m_1 \vec{x}_1 + m_3 \vec{x}_3}{m_1 + m_3} - \frac{m_2 \vec{x}_2 + m_4 \vec{x}_4}{m_2 + m_4}. \quad (38)$$

Obviously, with these sets of coordinates, the center-of-mass kinetic term T_{CM} can be completely eliminated for a nonrelativistic system. Besides, the Jacobi coordinates of Eq. (32) are also transformed with a common scaling angle θ .

A high-efficiency and exact method in solving the bound state of a few-body system, the GEM [69] is employed in this work; all of the relative motions of four-quark systems are expanded with various Gaussian basis which are taken as the geometric progression sizes,¹ and the form of orbital wave functions, ϕ 's in Eq. (32), is

$$\phi_{nlm}(\vec{r} e^{i\theta}) = N_{nl} (r e^{i\theta})^l e^{-\nu_n (r e^{i\theta})^2} Y_{lm}(\hat{r}). \quad (39)$$

Moreover, our present study is only in the S -wave state of double-heavy tetraquarks; no laborious Racah algebra during matrix element calculation for the value of the

spherical harmonic function is a constant when $l = 0$, i.e., $Y_{00} = \sqrt{1/4\pi}$.

Finally, in order to fulfill the Pauli principle, the complete wave function is written as

$$\Psi_{JM_J, I, i, j, k}(\theta) = \mathcal{A}[[\psi_L(\theta) \chi_S^{\sigma_i}(4)]_{JM_J} \chi_I^f \chi_k^c], \quad (40)$$

where \mathcal{A} is the antisymmetry operator of double-heavy tetraquarks by considering the nature of identical particle interchange ($\bar{q}\bar{q}$, cc , and bb). This is necessary, for the complete wave function of the four-quark system is constructed from two subclusters, i.e., meson-meson and diquark-antidiquark structures. In particular, when the two heavy quarks are of the same flavor ($QQ = cc$ or bb), the definitions of these two configurations in Fig. 2 with the quark arrangements of $\bar{q}Q\bar{q}Q$ are both

$$\mathcal{A} = 1 - (13) - (24) + (13)(24). \quad (41)$$

However, due to the asymmetry between c and b quarks, it is only two terms for $\bar{q}c\bar{q}b$ system and reads as

$$\mathcal{A} = 1 - (13). \quad (42)$$

III. RESULTS

In the present work, we systematically investigate the low-lying S -wave states of $QQ\bar{q}\bar{q}$ ($q = u, c$ and $Q = c, b$) tetraquarks in which both meson-meson and diquark-antidiquark configurations are considered. The parity for different double-heavy tetraquarks is positive under our assumption that the angular momenta l_1 , l_2 , and l_3 , which appear in Eq. (32), are all 0. In this way, the total angular momentum J coincides with the total spin S and can take values of 0, 1, and 2. All possible dimeson and diquark-antidiquark channels for $cc\bar{q}\bar{q}$, $bb\bar{q}\bar{q}$, and $cb\bar{q}\bar{q}$ systems are listed in Tables II–IV, respectively, and they have been grouped according to total spin parity J^P and isospin I . For clarity, the third and fifth columns of these tables show the necessary basis combination in spin ($\chi_j^{\sigma_i}$), flavor (χ_I^f), and color (χ_k^c) degrees of freedom. The physical channels with color-singlet (labeled with the superindex 1), hidden-color (labeled with the superindex 8), and diquark-antidiquark [labeled with $(QQ)(\bar{q}\bar{q})$] configurations are listed in the fourth and sixth columns.

Tables V–XVI summarize our calculated results (mass, size, and component) of possible lowest-lying double-heavy tetraquarks. In particular, Tables VI, IX, and XIV list each component of possible bound states of double-charm, double-bottom, and charm-bottom tetraquarks in the complete coupled-channel calculation in which all possible channels for a given quantum number IJ^P are considered. Their inner structures and the distance among any quark pair is shown in Tables VII, X, and XV; this is in order to get some insight about either molecular or compact

¹The details on Gaussian parameters can be found in Ref. [82].

TABLE II. All possible channels for $cc\bar{q}\bar{q}$ ($q = u$ or d) tetraquark systems.

J^P	Index	$I = 0$		$I = 1$	
		$\chi_J^{\sigma_i}; \chi_I^{f_j}; \chi_k^c [i; j; k]$	Channel	$\chi_J^{\sigma_i}; \chi_I^{f_j}; \chi_k^c [i; j; k]$	Channel
0^+	1	[1;1;1]	$(D^+D^0)^1$	[1;1;1]	$(D^0D^0)^1$
	2	[2;1;1]	$(D^{*+}D^{*0})^1$	[2;1;1]	$(D^{*0}D^{*0})^1$
	3	[1;1;2]	$(D^+D^0)^8$	[1;1;2]	$(D^0D^0)^8$
	4	[2;1;2]	$(D^{*+}D^{*0})^8$	[2;1;2]	$(D^{*0}D^{*0})^8$
	5			[3;1;4]	$(cc)(\bar{u}\bar{u})$
	6			[4;1;3]	$(cc)^*(\bar{u}\bar{u})^*$
1^+	1	[1;1;1]	$(D^+D^{*0})^1$	[1;1;1]	$(D^0D^{*0})^1$
	2	[3;1;1]	$(D^{*+}D^{*0})^1$	[3;1;1]	$(D^{*0}D^{*0})^1$
	3	[1;1;2]	$(D^+D^{*0})^8$	[1;1;2]	$(D^0D^{*0})^8$
	4	[3;1;2]	$(D^{*+}D^{*0})^8$	[3;1;2]	$(D^{*0}D^{*0})^8$
	5	[4;1;3]	$(cc)^*(\bar{u}\bar{d})$	[6;1;3]	$(cc)^*(\bar{u}\bar{u})^*$
	6	[5;1;4]	$(cc)(\bar{u}\bar{d})^*$		
2^+	1	[1;1;1]	$(D^{*+}D^{*0})^1$	[1;1;1]	$(D^{*0}D^{*0})^1$
	2	[1;1;2]	$(D^{*+}D^{*0})^8$	[1;1;2]	$(D^{*0}D^{*0})^8$
	3			[1;1;3]	$(cc)^*(\bar{u}\bar{u})^*$

tetraquark we are dealing with. The remaining tables below are of the calculated masses of these bound or resonance states of double-heavy tetraquarks; namely, Tables V and VIII present the results of double-charm and double-bottom tetraquarks whose quantum numbers are both of $I(J^P) = 0(1^+)$, and results on charm-bottom tetraquarks with $I(J^P) = 0(0^+)$, $0(1^+)$, and $0(2^+)$ are in Tables XI–XIII, respectively. Table XVI summarizes the obtained bound and resonance states of double-heavy tetraquarks in the complete coupled-channel calculation. Moreover, Figs. 3–7 present the distribution of complex energies of these

double-heavy tetraquarks in coupled-channel calculation by the complex scaling method. The transverse direction is of the real part of complex energy E , which stands for the mass of tetraquarks, and the longitudinal one is the imaginary part of E , which is related to the width, $\Gamma = -2\text{Im}(E)$. However, the other quantum states of each double-heavy tetraquark sector that do not appear here also have been considered in the calculation, but neither bound nor resonance states are found.

In Tables V, VIII, XI, XII, and XIII, the first column lists the physical channel of meson-meson and

TABLE III. All possible channels for $bb\bar{q}\bar{q}$ ($q = u$ or d) tetraquark systems.

J^P	Index	$I = 0$		$I = 1$	
		$\chi_J^{\sigma_i}; \chi_I^{f_j}; \chi_k^c [i; j; k]$	Channel	$\chi_J^{\sigma_i}; \chi_I^{f_j}; \chi_k^c [i; j; k]$	Channel
0^+	1	[1;2;1]	$(B^-\bar{B}^0)^1$	[1;2;1]	$(B^-B^-)^1$
	2	[2;2;1]	$(B^{*-}\bar{B}^{*0})^1$	[2;2;1]	$(B^{*-}B^{*-})^1$
	3	[1;2;2]	$(B^-\bar{B}^0)^8$	[1;2;2]	$(B^-B^-)^8$
	4	[2;2;2]	$(B^{*-}\bar{B}^{*0})^8$	[2;2;2]	$(B^{*-}B^{*-})^8$
	5			[3;2;4]	$(bb)(\bar{u}\bar{u})$
	6			[4;2;3]	$(bb)^*(\bar{u}\bar{u})^*$
1^+	1	[1;2;1]	$(B^-\bar{B}^{*0})^1$	[1;2;1]	$(B^-B^{*-})^1$
	2	[3;2;1]	$(B^{*-}\bar{B}^{*0})^1$	[3;2;1]	$(B^{*-}B^{*-})^1$
	3	[1;2;2]	$(B^-\bar{B}^{*0})^8$	[1;2;2]	$(B^-B^{*-})^8$
	4	[3;2;2]	$(B^{*-}\bar{B}^{*0})^8$	[3;2;2]	$(B^{*-}B^{*-})^8$
	5	[4;2;3]	$(bb)^*(\bar{u}\bar{d})$	[6;2;3]	$(bb)^*(\bar{u}\bar{u})^*$
	6	[5;2;4]	$(bb)(\bar{u}\bar{d})^*$		
2^+	1	[1;2;1]	$(B^{*-}\bar{B}^{*0})^1$	[1;2;1]	$(B^{*-}B^{*-})^1$
	2	[1;2;2]	$(B^{*-}\bar{B}^{*0})^8$	[1;2;2]	$(B^{*-}B^{*-})^8$
	3			[1;2;3]	$(bb)^*(\bar{u}\bar{u})^*$

TABLE IV. All possible channels for $cb\bar{q}\bar{q}$ ($q = u$ or d) tetraquark systems. For brevity, only the $D^{(*)0}B^{(*)0}$ structures are listed, and the corresponding $D^{(*)+}\bar{B}^{(*)-}$ ones are absent in $I = 0$. However, all these configurations are still employed in constructing the wave functions of four-quark systems.

J^P	Index	$I = 0$		$I = 1$	
		$\chi_J^{\sigma_i}; \chi_I^f; \chi_k^c [i; j; k]$	Channel	$\chi_J^{\sigma_i}; \chi_I^f; \chi_k^c [i; j; k]$	Channel
0^+	1	[1;3;1]	$(D^0\bar{B}^0)^1$	[1;3;1]	$(D^0B^-)^1$
	2	[2;3;1]	$(D^{*0}\bar{B}^{*0})^1$	[2;3;1]	$(D^{*0}B^{*-})^1$
	3	[1;3;2]	$(D^0\bar{B}^0)^8$	[1;3;2]	$(D^0B^-)^8$
	4	[2;3;2]	$(D^{*0}\bar{B}^{*0})^8$	[2;3;2]	$(D^{*0}B^{*-})^8$
	5	[3;3;3]	$(cb)(\bar{u}\bar{d})$	[3;3;4]	$(cb)(\bar{u}\bar{u})$
	6	[4;3;4]	$(cb)^*(\bar{u}\bar{d})^*$	[4;3;3]	$(cb)^*(\bar{u}\bar{u})^*$
1^+	1	[1;3;1]	$(D^0\bar{B}^{*0})^1$	[1;3;1]	$(D^0B^{*-})^1$
	2	[2;3;1]	$(D^{*0}\bar{B}^0)^1$	[2;3;1]	$(D^{*0}B^-)^1$
	3	[3;3;1]	$(D^{*0}\bar{B}^{*0})^1$	[3;3;1]	$(D^{*0}B^{*-})^1$
	4	[1;3;2]	$(D^0\bar{B}^{*0})^8$	[1;3;2]	$(D^0B^{*-})^8$
	5	[2;3;2]	$(D^{*0}\bar{B}^0)^8$	[2;3;2]	$(D^{*0}B^-)^8$
	6	[3;3;2]	$(D^{*0}\bar{B}^{*0})^8$	[3;3;2]	$(D^{*0}B^{*-})^8$
	7	[4;3;3]	$(cb)^*(\bar{u}\bar{d})$	[4;3;4]	$(cb)^*(\bar{u}\bar{u})$
	8	[5;3;4]	$(cb)(\bar{u}\bar{d})^*$	[5;3;3]	$(cb)(\bar{u}\bar{u})^*$
	9	[6;3;4]	$(cb)^*(\bar{u}\bar{d})^*$	[6;3;3]	$(cb)^*(\bar{u}\bar{u})^*$
2^+	1	[1;3;1]	$(D^{*0}\bar{B}^{*0})^1$	[1;3;1]	$(D^{*0}B^{*-})^1$
	2	[1;3;2]	$(D^{*0}\bar{B}^{*0})^8$	[1;3;2]	$(D^{*0}B^{*-})^8$
	3	[1;3;4]	$(cb)^*(\bar{u}\bar{d})^*$	[1;3;3]	$(cb)^*(\bar{u}\bar{u})^*$

TABLE V. Lowest-lying states of double-charm tetraquarks with quantum numbers $I(J^P) = 0(1^+)$, units in MeV.

Channel	Color	M	E_B	M'
D^+D^{*0} (3877)	S	3915	0	3877
	H	4421	+506	4383
	S + H	3914	-1	3876
Percentage (S;H): 97.3%; 2.7%				
$D^{*+}D^{*0}$ (4018)	S	4034	0	4018
	H	4390	+356	4374
	S + H	4033	-1	4017
Percentage (S;H): 95.5%; 4.5%				
$(cc)^*(\bar{u}\bar{d})$		3778		
$(cc)(\bar{u}\bar{d})^*$		4220		
Mixed		3726		

TABLE VI. Component of each channel in coupled-channel calculation with $IJ^P = 01^+$; the numbers 1 and 8 in superscript are for the singlet-color and hidden-color channel, respectively.

$(D^+D^{*0})^1$	$(D^{*+}D^{*0})^1$	$(D^+D^{*0})^8$	$(D^{*+}D^{*0})^8$
25.8%	15.4%	10.7%	11.2%
$(cc)^*(\bar{u}\bar{d})$ 36.7%	$(cc)(\bar{u}\bar{d})^*$ 0.2%		

TABLE VII. The distance, in femtometers, between any two quarks of the found tetraquark bound states in coupled-channel calculation ($q = u, d$).

$r_{\bar{u}\bar{d}}$	$r_{\bar{q}c}$	r_{cc}
0.658	0.666	0.522

TABLE VIII. Lowest-lying states of double-bottom tetraquarks with quantum numbers $I(J^P) = 0(1^+)$, units in MeV.

Channel	Color	M	E_B	M'
$B^-\bar{B}^{*0}$ (10604)	S	10585	-12	10592
	H	10987	+390	10994
	S + H	10562	-35	10569
Percentage (S;H): 83.0%; 17.0%				
$B^{*-}\bar{B}^{*0}$ (10650)	S	10627	-11	10639
	H	10974	+336	10986
	S + H	10601	-37	10613
Percentage (S;H): 79.6%; 20.4%				
$(bb)^*(\bar{u}\bar{d})$		10261		
$(bb)(\bar{u}\bar{d})^*$		10787		
Mixed		10238 ^{1st}		
		10524 ^{2nd}		

TABLE IX. Component of each channel in coupled-channel calculation with $IJ^P = 01^+$; the numbers 1 and 8 in superscript are for the singlet-color and hidden-color channel, respectively.

	$(B^-\bar{B}^{*0})^1$	$(B^{*-}\bar{B}^{*0})^1$	$(B^-\bar{B}^{*0})^8$
1st	20.7%	17.9%	9.3%
2nd	25.6%	14.8%	9.5%
	$(B^{*-}\bar{B}^{*0})^8$	$(bb)^*(\bar{u}\bar{d})$	$(bb)(\bar{u}\bar{d})^*$
1st	9.4%	42.6%	0.1%
2nd	9.1%	40.2%	0.8%

TABLE X. The distance, in femtometers, between any two quarks of the found tetraquark bound states in coupled-channel calculation ($q = u, d$).

	$r_{\bar{u}\bar{d}}$	$r_{\bar{q}b}$	r_{bb}
1st	0.604	0.608	0.328
2nd	0.830	0.734	0.711

TABLE XI. Lowest-lying states of charm-bottom tetraquarks with quantum numbers $I(J^P) = 0(0^+)$, unit in MeV.

Channel	Color	M	E_B	M'
$D^0\bar{B}^0$ (7147)	S	7172	-4	7143
	H	7685	+509	7656
	S + H	7171	-5	7142
Percentage (S;H): 96.4%; 3.6%				
$D^{*0}\bar{B}^{*0}$ (7334)	S	7327	-9	7325
	H	7586	+250	7584
	S + H	7297	-39	7295
Percentage (S;H): 87.8%; 12.2%				
$(cb)(\bar{u}\bar{d})$		7028		
$(cb)^*(\bar{u}\bar{d})^*$		7482		
Mixed		6980		

TABLE XII. Lowest-lying states of charm-bottom tetraquarks with quantum numbers $I(J^P) = 0(1^+)$, units in MeV.

Channel	Color	M	E_B	M'
$D^0\bar{B}^{*0}$ (7193)	S	7214	-3	7190
	H	7694	+477	7670
	S + H	7213	-4	7189
Percentage (S;H): 96.8%; 3.2%				
$D^{*0}\bar{B}^0$ (7288)	S	7293	-2	7286
	H	7707	+412	7700
	S + H	7292	-3	7285
Percentage (S;H): 96.8%; 3.2%				
$D^{*0}\bar{B}^{*0}$ (7334)	S	7334	-2	7332
	H	7691	+354	7688
	S + H	7326	-10	7324

(Table continued)

TABLE XII. (Continued)

Channel	Color	M	E_B	M'
Percentage (S;H): 89.3%; 10.7%				
$(cb)^*(\bar{u}\bar{d})$		7039		
$(cb)(\bar{u}\bar{d})^*$		7531		
$(cb)^*(\bar{u}\bar{d})^*$		7507		
Mixed		6997		

TABLE XIII. Lowest-lying states of charm-bottom tetraquarks with quantum numbers $I(J^P) = 0(2^+)$, units in MeV.

Channel	Color	M	E_B	M'
$D^{*0}\bar{B}^{*0}$ (7334)	S	7334	-2	7332
	H	7720	+384	7718
	S + H	7334	-2	7332
Percentage (S;H): 99.8%; 0.2%				
$(cb)^*(\bar{u}\bar{d})^*$		7552		
Mixed		7333		

TABLE XIV. Component of each channel in coupled-channel calculation; the numbers 1 and 8 in superscript are for the singlet-color and hidden-color channel, respectively ($q = u, d$).

IJ^P	$(D^0\bar{B}^0)^1$	$(D^{*0}\bar{B}^{*0})^1$	$(D^0\bar{B}^0)^8$	$(D^{*0}\bar{B}^{*0})^8$
00^+	26.4%	21.5%	1.6%	1.9%
	$(cb)(\bar{u}\bar{d})$ 48.5%	$(cb)^*(\bar{u}\bar{d})^*$ 0.1%		
01^+	$(D^0\bar{B}^0)^1$ 20.2%	$(D^{*0}\bar{B}^0)^1$ 11.6%	$(D^{*0}\bar{B}^{*0})^1$ 16.8%	$(D^0\bar{B}^{*0})^8$ 1.4%
	$(D^{*0}\bar{B}^0)^8$ 1.3%	$(D^{*0}\bar{B}^{*0})^8$ 1.8%	$(cb)^*(\bar{u}\bar{d})$ 46.4%	$(cb)(\bar{u}\bar{d})^*$ 0.1%
	$(cb)^*(\bar{u}\bar{d})^*$ 0.4%			
02^+	$(D^{*0}\bar{B}^{*0})^1$ 98.6%	$(D^{*0}\bar{B}^{*0})^8$ 0.3%	$(cb)^*(\bar{u}\bar{d})^*$ 1.1%	

diquark-antidiquark (if it fulfills the Pauli principle), and the experimental value of the noninteracting meson-meson threshold is also indicated in parentheses; the second column refers to color-singlet (S), hidden-color (H), and

TABLE XV. The distance, in femtometers, between any two quarks of the found tetraquark bound states in coupled-channel calculation ($q = u, d$).

IJ^P	$r_{\bar{u}\bar{d}}$	$r_{\bar{q}c}$	$r_{\bar{q}b}$	r_{cb}
00^+	0.635	0.653	0.610	0.428
01^+	0.632	0.661	0.616	0.434
02^+	2.248	1.612	1.597	2.102

TABLE XVI. Possible bound and resonance states for $QQ\bar{q}\bar{q}$ ($q = u$ or d) tetraquarks in the CSM with rotated angle θ varying from 0° to 6° . The imaginary part of the complex energy and resonance width are with the relation of $\text{Im}(E) = -\Gamma/2$, units in MeV.

		0°	2°	4°	6°
$cc\bar{q}\bar{q}$	Bound state	3726	3726	3726	3726
$IJ^P = 01^+$	Resonance state	...	$4319 - 7.9i$	$4312 - 9.4i$	$4310 - 7.3i$
$bb\bar{q}\bar{q}$	Bound state	10238; 10524	10238; 10524	10238; 10524	10238; 10524
$IJ^P = 01^+$	Resonance state	...	$10814 - 0.9i$	$10814 - 1.1i$	$10814 - 1.0i$
$cb\bar{q}\bar{q}$	Bound state	6980	6980	6980	6980
$IJ^P = 00^+$	Resonance state	...	$7722 - 6.5i$	$7726 - 6.1i$	$7728 - 5.2i$
$cb\bar{q}\bar{q}$	Bound state	6997	6997	6997	6997
$IJ^P = 01^+$	Resonance state	...	$7327 - 1.0i$	$7327 - 1.2i$	$7327 - 1.3i$
$cb\bar{q}\bar{q}$	Bound state	7333	7333	7333	7333
$IJ^P = 02^+$	Resonance state

coupled-channel (S + H) calculations for the meson-meson configuration; the following two columns show the theoretical mass (M) and binding energy (E_B) of the tetraquark state; moreover, to avoid theoretical uncertainties coming from the quark model prediction of the meson spectra, the last column presents the rescaled theoretical mass (M') of the tetraquark state by attending to the corresponding experimental meson-meson threshold.

Now let us proceed to describe in detail our theoretical findings for each sector of double-heavy tetraquarks.

A. Double-charm tetraquarks

In this sector, the bound state and resonance are found only in the $I(J^P) = 0(1^+)$ state. Two possible meson-meson channels, D^+D^{*0} and $D^{*+}D^{*0}$, along with two diquark-antidiquark channels, $(cc)^*(\bar{u}\bar{d})$ and $(cc)(\bar{u}\bar{d})^*$, are studied in Table V. It is obvious to notice that there is no bound state in either color-singlet (S) or hidden-color channels (H) of the meson-meson configuration. However, this result is reversed by their coupled-channel calculation (S + H), and there are -1 MeV weakly binding energies for both D^+D^{*0} and $D^{*+}D^{*0}$ channels. After corrections, the rescaled masses of these two channels are 3876 and 4017 MeV, respectively. Meanwhile, the nature of molecular-type $D^{(*)+}D^{*0}$ structures are shown up, since the color-singlet channel contributions are more than 95%.

In contrast to the weakly bound states around the $D^{(*)+}D^{*0}$ thresholds, there is almost -140 MeV binding energy for the $(cc)^*(\bar{u}\bar{d})$ channel when compared with the theoretical threshold of D^+D^{*0} . However, the other diquark-antidiquark channel $(cc)(\bar{u}\bar{d})^*$ is above the D^+D^{*0} and $D^{*+}D^{*0}$ theoretical thresholds with $E_B = +305$ and $+186$ MeV, respectively. This deeply bound diquark-antidiquark state $(cc)^*(\bar{u}\bar{d})$ motivates a further complete coupled-channel calculation in which all the color-singlet, hidden-color meson-meson channels and diquark-antidiquark ones are considered. The obtained mass is

3726 MeV, which is 52 MeV lower than the single-channel result of $(cc)^*(\bar{u}\bar{d})$; besides, the nature of the compact double-charm tetraquark state is clearly presented in Table VII, where the distance between any two quarks is calculated and the obtained size of this four-quark system is less than 0.67 fm. Table VI shows each component in the coupled-channel calculation. In particular, two mainly comparable components, color-singlet channel D^+D^{*0} (25.8%) and the $(cc)^*(\bar{q}\bar{q})$ one (36.7%), are consistent with our result of strong coupling effect and compact tetraquark structure.

The obtained deeply bound double-charm tetraquark with $M = 3726$ MeV by CSM in the complete coupled-channel calculation is clearly shown in Fig. 3. We vary the rotated angle θ from 0° to 6° , and this bound state remains on the real axis. Particularly, the black dots in the real axis are the calculated masses in coupled-channel calculation with $\theta = 0^\circ$, and the red, blue, and green ones are for

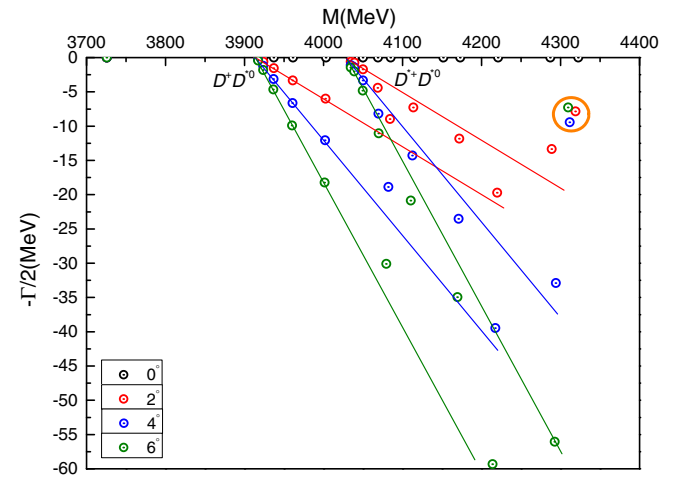


FIG. 3. Complex energies of double-charm tetraquarks with $IJ^P = 01^+$ in the coupled-channel calculation, θ varying from 0° to 6° .

complex energies with $\theta = 2^\circ$, 4° , and 6° , respectively. Generally, they are aligned along the threshold lines with the same color, and the nature of the scattering state of D^+D^{*0} and $D^{*+}D^{*0}$ in coupled channels is clear, for their calculated poles always move along the cut lines when the scaling angle θ changes. However, there is a mismatch between the calculated dots and threshold lines in the high-energy region with a large width. Nevertheless, we mainly focus on the low-lying state in this work, and those calculation noises still present the nature of scattering states with an obviously moving track.

In Fig. 3, one can see that there is a possible resonance pole marked with an orange circle above the nearer $D^{*+}D^{*0}$ threshold lines. The three dots obtained by the CSM calculation with $\theta = 2^\circ$, 4° , and 6° , respectively, are located in a quite small energy region. Their complex energies are listed in Table XVI, and the estimated resonance mass and width are ~ 4312 MeV and ~ 16 MeV, respectively. By considering the fact that the resonance pole is nearer $D^{*+}D^{*0}$ threshold lines than D^+D^{*0} , hence the former channel should play a more important role in this resonance state.

B. Double-bottom tetraquarks

We herein investigate $B^{(*)-}\bar{B}^{*0}$ and $(bb)^*(\bar{u}\bar{d})^{(*)}$ channels which are similar to the double-charm tetraquarks. Possible bound and resonance states are also obtained only in the $I(J^P) = 0(1^+)$ state. However, with much heavier b -flavored quarks included, possible bound states of color-singlet channels of $B^-\bar{B}^{*0}$ and $B^{*-}\bar{B}^{*0}$ are found; their binding energies are -12 and -11 MeV, respectively. Additionally, in Table VIII, one can find that nearly triple binding energies are obtained for both $B^-\bar{B}^{*0}$ ($E_B = -35$ MeV) and $B^{*-}\bar{B}^{*0}$ ($E_B = -37$ MeV) when the hidden-color channels are incorporated in the calculation. These deeper bound states than $D^{(*)+}D^{*0}$ cases also indicate a strong coupling which is about 80% color-singlet component for $B^{(*)-}\bar{B}^{*0}$. After a mass shift for these two bound states, the slightly modified masses of double-bottom tetraquarks are 10569 and 10613 MeV, respectively.

In the diquark-antidiquark configuration, according to the $B^-\bar{B}^{*0}$ theoretical thresholds, one tightly bound state of $(bb)^*(\bar{u}\bar{d})$ whose binding energy is $E_B = -336$ MeV and one excited state of $(bb)(\bar{u}\bar{d})^*$ with $E_B = +190$ MeV are shown in Table VIII, respectively. This situation is also consistent with $(cc)^*(\bar{u}\bar{d})^{(*)}$ channels which are of smaller binding energies. The obtained deeply bound state $(bb)^*(\bar{u}\bar{d})$ at 10261 MeV is supported by Refs. [52,53,55,56], only ~ 130 MeV lower than the predicted mass in Ref. [53].

Furthermore, two bound states are found in a coupled-channel calculation in which all the channels listed in Table VIII are considered; their masses are 10238

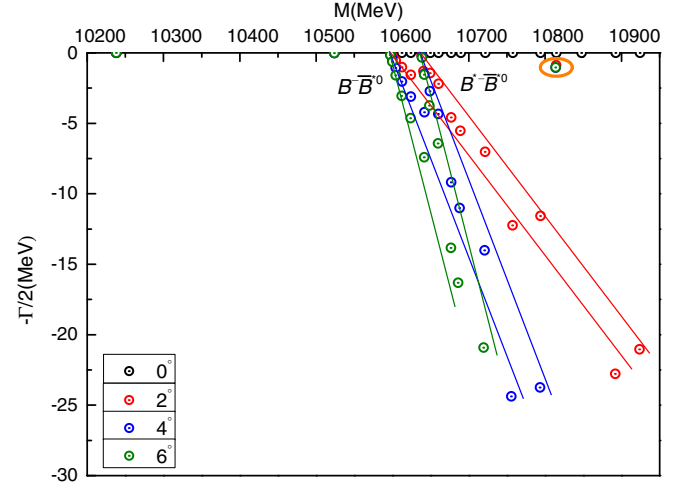


FIG. 4. Complex energies of double-bottom tetraquarks with $IJ^P = 01^+$ in the coupled-channel calculation, θ varying from 0° to 6° .

and 10524 MeV, respectively. Clearly, the $(bb)^*(\bar{u}\bar{d})$ diquark-antidiquark channel is pushed down by 23 MeV due to the coupling effect, and the second bound state ($M = 10524$ MeV) is 73 MeV below the $B^-\bar{B}^{*0}$ theoretical threshold. Then with a purpose of disentangling the nature of these two obtained bound states, their components and inner structures are studied. One can see in Table IX that the components of the two bound states are quite comparable and both about 42% for the $(bb)^*(\bar{u}\bar{d})$ channel and about 20% subdominant for the color-singlet channel of $B^{(*)-}\bar{B}^{*0}$. With no more than 0.83 fm distance for any quark pair listed in Table X, the compact tetraquark structures for these two bound states are clearly presented again, and one needs to mention that the distances of two bottom quarks for them are only 0.328 and 0.711 fm, respectively.

In Table XVI and Fig. 4, one can find that the two bound states are stable against the change of scaling angle θ . Besides, one resonance state whose mass and width are 10814 and 2 MeV, respectively, is obtained in the complete coupled-channel calculation with various rotated angles θ . We mark it with a big orange circle, where the three dots almost overlap and their complex energies within θ taking the value of 2° , 4° , and 6° are listed in Table XVI, respectively. This narrow width resonance pole is close to the $B^{*-}\bar{B}^{*0}$ threshold line, and more contributions should be made by this channel. However, the other poles with a scattering nature are generally aligned along the $B^-\bar{B}^{*0}$ and $B^{*-}\bar{B}^{*0}$ threshold lines.

C. Charm-bottom tetraquarks

In these sector, some bound or resonance states are obtained only for isoscalar tetraquarks, and our theoretical findings in meson-meson channels are comparable with those results in Table V of Ref. [94]. Hence, we will discuss them according to $I(J^P)$ quantum numbers individually.

1. The $I(J^P)=0(0^+)$ channel

Loosely bound states of the color-singlet channel of $D^0\bar{B}^0$ and $D^{*0}\bar{B}^{*0}$ are found; their binding energies are -4 and -9 MeV, respectively. In Table XI, one can realize that there is only a remarkable coupling effect ($E_B = -39$ MeV) on the $D^{*0}\bar{B}^{*0}$ configuration when the hidden-color channel is incorporated, and almost no influence on the $D^0\bar{B}^0$ channel with only 1 MeV binding energy increased. This is supported by our calculated proportion for color-singlet and hidden-color channels: 96.4% for $(D^0\bar{B}^0)^1$ and 87.8% for $(D^{*0}\bar{B}^{*0})^1$. Meanwhile, one deeply bound state $(cb)(\bar{u}\bar{d})$ with $E_B = -148$ MeV and one excited state $(cb)^*(\bar{u}\bar{d})^*$ with $E_B = +306$ MeV are found with respect to the $D^0\bar{B}^0$ theoretical threshold. The binding energy of the lowest-lying state is increased by 48 MeV in the complete coupled-channel calculation. This tightly bound state whose mass is 6980 MeV brings us a compact double-heavy tetraquark structure again. Table XV presents the size of the state around 0.6 fm and an even smaller distance, 0.428 fm, for the cb quark pair. All of these features can be related to the strong coupling effect, which is almost 50% for $(cb)(\bar{u}\bar{d})$, 26.4% for $(D^0\bar{B}^0)^1$, and 21.5% for $(D^{*0}\bar{B}^{*0})^1$ channels, as shown in Table XIV.

In the complex scaling computation that the investigated region of rotated angle θ is the same as the previous two types of tetraquark states, the bound state along with a resonance is presented in Fig. 5. Specifically, four dots whose θ take the value of 0° , 2° , 4° , and 6° , respectively, overlap exactly at mass 6980 MeV on the real axis. The resonance pole is found near the mass of 7726 MeV, and its width is ~ 12 MeV according to Table XVI. Moreover, one can find in Fig. 5 that the resonance state is far from the $D^0\bar{B}^0$ threshold, and, accordingly, the majority contributions should owe to the $D^{*0}\bar{B}^{*0}$ channel.

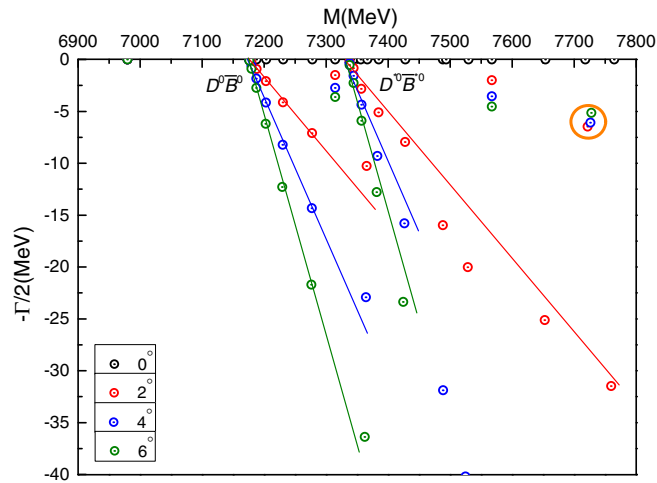


FIG. 5. Complex energies of charm-bottom tetraquarks with $IJ^P = 00^+$ in the coupled-channel calculation, θ varying from 0° to 6° .

The rest of the calculated poles in Fig. 5 are basically fit well with the $D^0\bar{B}^0$ and $D^{*0}\bar{B}^{*0}$ threshold lines, except for two cases. Namely, the dots always descend slowly with the increasing of scaling angle θ at both mass 7314 and 7567 MeV. They cannot be identified as resonance states due to the instability.

2. The $I(J^P)=0(1^+)$ channel

All three channels in meson-meson $D^{(*)0}\bar{B}^{(*)0}$ and diquark-antidiquark $(cb)^*(\bar{u}\bar{d})^*$ configurations are studied in Table XII. Four similar features as the other double-heavy tetraquarks discussed before can be drawn: (i) loosely bound states with $E_B = -3$, -2 , and -2 MeV for the three color-singlet channels of $D^0\bar{B}^0$, $D^{*0}\bar{B}^0$, and $D^{*0}\bar{B}^{*0}$, respectively; (ii) the coupling between color-singlet and hidden-color channels is quite weak (E_B increased by 1 MeV) for $D^0\bar{B}^0$ and $D^{*0}\bar{B}^0$ configurations, but 8 MeV increased binding energy for $D^{*0}\bar{B}^{*0}$; (iii) only one deeply bound state in the single-channel calculation, namely, $E_B = -178$ MeV for the $(cb)^*(\bar{u}\bar{d})$ channel when compared with the lowest theoretical threshold of $D^0\bar{B}^0$; and (iv) a more tightly bound state whose mass is 6997 MeV in the complete coupled-channel calculation.

In Table XIV, one can see that the most contribution 46.4% comes from the $(cb)^*(\bar{u}\bar{d})$ channel, and the other three subdominant channels are 20.2% for $(D^0\bar{B}^{*0})^1$, 11.6% for $(D^{*0}\bar{B}^0)^1$, and 16.8% for $(D^{*0}\bar{B}^{*0})^1$. These facts of the strong coupling effect along with the domination of the diquark-antidiquark configuration result in a compact structure again, and one can find a comparable size between $IJ^P = 01^+$ and 00^+ state in Table XV.

Figure 6 presents the distribution of complex energies in the complete coupled-channel calculation. Three scattering states of $D^0\bar{B}^0$, $D^{*0}\bar{B}^0$, and $D^{*0}\bar{B}^{*0}$ are clearly shown, and the bound state whose mass is 6997 MeV remains on the

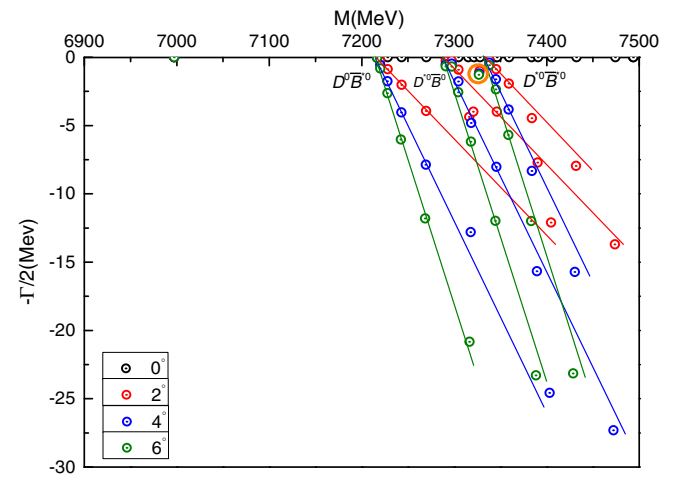


FIG. 6. Complex energies of charm-bottom tetraquarks with $IJ^P = 01^+$ in the coupled-channel calculation, θ varying from 0° to 6° .

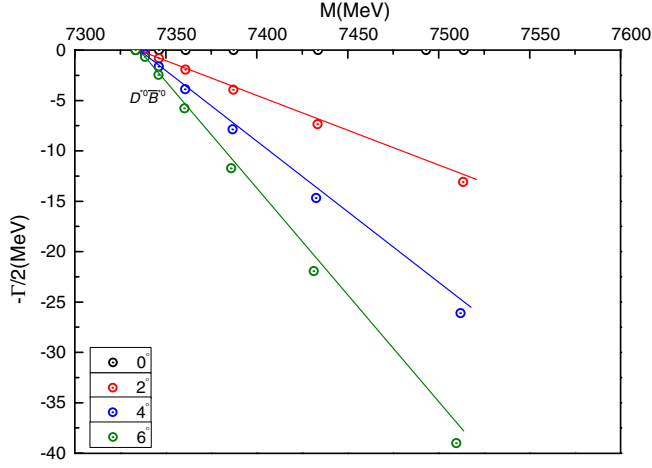


FIG. 7. Complex energies of charm-bottom tetraquarks with $IJ^P = 02^+$ in the coupled-channel calculation, θ varying from 0° to 6° .

real axis. Meanwhile, one narrow width resonance state as double-bottom tetraquarks whose $\Gamma = 2$ MeV is obtained and marked with a orange circle in the figure. $D^{*0}\bar{B}^0$ and $D^{*0}\bar{B}^{*0}$ channels should both be important to this quite narrow resonance pole which is among the threshold lines of them. The resonance mass is 7327 MeV, and its width is ~ 2.4 MeV in the CSM computation with θ varying from 0° to 6° in Table XVI.

3. The $I(J^P) = 0(2^+)$ channel

Only two channels contribute to this case: the $D^{*0}\bar{B}^{*0}$ meson-meson channel and the diquark-antidiquark one $(cb)^*(\bar{u}\bar{d})^*$. As in all cases studied before, a loosely bound state of color-singlet channel $D^{*0}\bar{B}^{*0}$ is obtained with $E_B = -2$ MeV. Furthermore, the coupling is still quite weak in the complete coupled-channel investigation, for the $(D^{*0}\bar{B}^{*0})^1$ channel contributes 98.6%, and the calculated mass is 7333 MeV, which is quite close to the color-singlet channel one of 7334 MeV. This indicates the nature of molecular-type meson-meson structure, and it is also consistent with the obtained size in Table XV, where the distances between any two quarks are about 1.6–2.2 fm.

In additional, no resonance state is found in the complete coupled-channel calculation with θ varying from 0° to 6° . The loosely bound state with $M = 7333$ MeV and another scattering state of $D^{*0}\bar{B}^{*0}$ are presented in Fig. 7, respectively.

IV. EPILOGUE

In a complex scaling range of the chiral quark formalism, by considering meson-meson and diquark-antidiquark configurations along with all color structures (couplings are also considered), i.e., color-singlet and hidden-color channels for dimeson structure and color triplet-antitriplet

and sextet-antisextet channels for $(QQ)(\bar{q}\bar{q})$ structure, we have studied the possibility of having tetraquark bound and resonance states in the double-heavy sectors with quantum numbers $J^P = 0^+, 1^+$, and 2^+ and in the 0 and 1 isospin sectors. For possible bound states in the complete coupled-channel study, their inner structures and components are also analyzed by computing the distances among any pair of quarks and the contributions of each channel's wave functions. Masses and widths for possible resonance states are also calculated in the coupled-channel calculation. The model parameters which are included in the perturbative one-gluon exchange, the nonperturbative linear-screened confining, and Goldstone-boson exchange interactions between light quarks have been fitted in the past through hadron, hadron-hadron, and multi-quark phenomenology.

For all quantum states of the investigated double-heavy tetraquarks, $cc\bar{q}\bar{q}$, $bb\bar{q}\bar{q}$, and $cb\bar{q}\bar{q}$ ($q = u, d$), tightly bound and narrow resonance states are obtained only in the $IJ^P = 01^+$ state for the former two sectors, and they are also obtained for $cb\bar{q}\bar{q}$ in 00^+ and 01^+ states. However, only a loosely bound state is found for charm-bottom tetraquarks in 02^+ states. All of these states within meson-meson configurations are loosely bound whether in color-singlet channels or coupling to hidden-color ones. However, compact structures are available in diquark-antidiquark channels except for charm-bottom tetraquarks in 02^+ states. Let us characterize the features in detail.

First, in double-charm tetraquark states, two loosely bound states D^+D^{*0} and $D^{*+}D^{*0}$ with mass 3876 and 4017 MeV, respectively, are obtained in the $IJ^P = 01^+$ state. Meanwhile, a deeply bound state with $(cc)^*(\bar{u}\bar{d})$ diquark-antidiquark structure is found at 3778 MeV. In the complete coupled-channel calculation, the lowest-lying state mass is 3726 MeV, and the compact tetraquark state size is 0.52–0.66 fm. Meanwhile, a resonance state which is mainly induced by the $D^{*+}D^{*0}$ channel is obtained, and the estimated mass and width are 4312 and 16 MeV, respectively.

Second, similar to the double-charm tetraquarks, we found loosely bound states of $B^-\bar{B}^{*0}$ and $B^{*-}\bar{B}^{*0}$ with $IJ^P = 01^+$; the predicted masses are 10569 and 10613 MeV, respectively. There are $\sim 20\%$ contributions from hidden-color channels for these two molecular states. Diquark-antidiquark state $(bb)^*(\bar{u}\bar{d})$ is much more tightly bound with a binding energy $E_B = -336$ MeV when compared with the theoretical threshold of the $B^-\bar{B}^{*0}$ channel. In the complete coupled-channel calculation, two compact tetraquark bound states with a mass at 10238 and 10524 MeV, respectively, are obtained. The distances among any quark pair of them are less than 0.83 fm. Besides, a narrow resonance state with mass $M = 10814$ MeV and width $\Gamma = 2$ MeV is found, and the $B^{*-}\bar{B}^{*0}$ channel plays an important role to this state.

In additional, possible charm-bottom tetraquark states are found in three quantum states $IJ^P = 00^+, 01^+$, and 02^+ . Specifically, in the 00^+ state, $D^0\bar{B}^0(7142)$ and

$D^{*0}\bar{B}^{*0}(7295)$; in the 01^+ state, $D^0\bar{B}^{*0}(7189)$, $D^{*0}\bar{B}^0(7285)$, and $D^{*0}\bar{B}^{*0}(7324)$; and in the 02^+ state, $D^{*0}\bar{B}^{*0}(7332)$, the predicted masses for these molecular states are correspondingly signed in the brackets. The compact tetraquarks $(cb)(\bar{u}\bar{d})$ and $(cb)^*(\bar{u}\bar{d})$ with a mass at 7028 and 7039 MeV, respectively, are found in 00^+ and 01^+ states, respectively. In the complete coupled-channel calculation, these two states are of lower masses 6980 and 6997 MeV; besides, their sizes are both less than 0.67 fm. However, the 02^+ state remains the molecular-type structure due to quite weak coupling. Two resonances are available for 00^+ and 01^+ states; their mass and width are 7726 and 12 MeV and 7327 and 2.4 MeV, respectively. The $D^{*0}\bar{B}^{*0}$ channel is crucial for the resonance state with $IJ^P = 00^+$, and resonance in the 01^+ state is mainly induced by $D^{*0}\bar{B}^0$ and $D^{*0}\bar{B}^{*0}$ channels.

Finally, our results in this work by the phenomenological framework of the chiral quark model are expected to be

confirmed in future high-energy experiments. Meanwhile, a natural extension of our investigation in a next step will be the other open-heavy tetraquark states, i.e., $QQ\bar{Q}\bar{q}$ systems. Properties in those almost nonrelativistic systems are also absorbing.

ACKNOWLEDGMENTS

G. Y. thanks L. He for his support and informative discussions. Work partially financed by China Postdoctoral Science Foundation Grant No. 2019M650617; National Natural Science Foundation of China under Grants No. 11535005, No. 11775118, No. 11890712, and No. 11775123; and Spanish Ministerio de Economía, Industria y Competitividad under Contract No. FPA2017-86380-P.

-
- [1] S. K. Choi *et al.* (LEPS Collaboration), *Phys. Rev. Lett.* **91**, 262001 (2003).
 - [2] D. Acosta *et al.* (CDF II Collaboration), *Phys. Rev. Lett.* **93**, 072001 (2004).
 - [3] V. M. Abazov *et al.* (D0 Collaboration), *Phys. Rev. Lett.* **93**, 162002 (2004).
 - [4] B. Aubert *et al.* (BABAR Collaboration), *Phys. Rev. D* **71**, 071103 (2005).
 - [5] S. Godfrey and N. Isgur, *Phys. Rev. D* **32**, 189 (1985).
 - [6] D. Ebert, R. N. Faustov, and V. O. Galkin, *Eur. Phys. J. C* **71**, 1825 (2011).
 - [7] J. Segovia, D. R. Entem, F. Fernandez, and E. Hernandez, *Int. J. Mod. Phys. E* **22**, 1330026 (2013).
 - [8] J. Vijande, F. Fernandez, and A. Valcarce, *J. Phys. G* **31**, 481 (2005).
 - [9] T. Barnes and S. Godfrey, *Phys. Rev. D* **69**, 054008 (2004).
 - [10] E. J. Eichten, K. Lane, and C. Quigg, *Phys. Rev. D* **69**, 094019 (2004).
 - [11] Y. Dong, A. Faessler, T. Gutsche, and V. E. Lyubovitskij, *Phys. Rev. D* **77**, 094013 (2008).
 - [12] Y. Dong, A. Faessler, T. Gutsche, S. Kovalenko, and V. E. Lyubovitskij, *Phys. Rev. D* **79**, 094013 (2009).
 - [13] D. Gamermann, J. Nieves, E. Oset, and E. R. Arriola, *Phys. Rev. D* **81**, 014029 (2010).
 - [14] F.-K. Guo, C. Hanhart, Y. S. Kalashnikova, U.-G. Meissner, and A. V. Nefediev, *Phys. Lett. B* **742**, 394 (2015).
 - [15] L. Maiani, F. Piccinini, A. D. Polosa, and V. Riquer, *Phys. Rev. D* **71**, 014028 (2005).
 - [16] P. G. Ortega, J. Segovia, D. R. Entem, and F. Fernández, *Phys. Rev. D* **81**, 054023 (2010).
 - [17] S. Coito, G. Rupp, and E. Beveren, *Eur. Phys. J. C* **71**, 1762 (2011).
 - [18] J. Ferretti, G. Galatà, and E. Santopinto, *Phys. Rev. D* **90**, 054010 (2014).
 - [19] M. Cardoso, G. Rupp, and E. Beveren, *Eur. Phys. J. C* **75**, 26 (2015).
 - [20] Y. Tan and J. Ping, *Phys. Rev. D* **100**, 034022 (2019).
 - [21] B. Aubert *et al.* (BABAR Collaboration), *Phys. Rev. Lett.* **95**, 142001 (2005).
 - [22] S.-K. Choi *et al.* (Belle Collaboration), *Phys. Rev. Lett.* **100**, 142001 (2008).
 - [23] T. Aaltonen *et al.* (CDF Collaboration), *Phys. Rev. Lett.* **102**, 242002 (2009).
 - [24] M. Ablikim *et al.* (BESIII Collaboration), *Phys. Rev. Lett.* **110**, 252001 (2013).
 - [25] R. Aaij *et al.* (LHCb Collaboration), *Phys. Rev. Lett.* **115**, 072001 (2015).
 - [26] R. Aaij *et al.* (LHCb Collaboration), *Phys. Rev. Lett.* **122**, 222001 (2019).
 - [27] H.-X. Chen, W. Chen, X. Liu, and S.-L. Zhu, *Phys. Rep.* **639**, 1 (2016).
 - [28] H.-X. Chen, W. Chen, X. Liu, Y.-R. Liu, and S.-L. Zhu, *Rep. Prog. Phys.* **80**, 076201 (2017).
 - [29] F.-K. Guo, C. Hanhart, Ulf-G. Meissner, Q. Wang, Q. Zhao, and B.-S. Zou, *Rev. Mod. Phys.* **90**, 015004 (2018).
 - [30] S. L. Olsen, T. Skwarnicki, and D. Zieminska, *Rev. Mod. Phys.* **90**, 015003 (2018).
 - [31] V. Khachatryan *et al.* (CMS Collaboration), *J. High Energy Phys.* **05** (2017) 013.
 - [32] L. C. Bland *et al.* (ANDY Collaboration), *arXiv:1909.03124*.
 - [33] R. Aaij *et al.* (LHCb Collaboration), *J. High Energy Phys.* **10** (2018) 086.
 - [34] A. V. Berezhnoy, A. V. Luchinsky, and A. A. Novoselov, *Phys. Rev. D* **86**, 034004 (2012).
 - [35] A. Esposito and A. D. Polosa, *Eur. Phys. J. C* **78**, 782 (2018).

- [36] M. N. Anwar, J. Ferretti, F.-K. Guo, E. Santopinto, and B.-S. Zou, *Eur. Phys. J. C* **78**, 647 (2018).
- [37] M. A. Bedolla, J. Ferretti, C. D. Roberts, and E. Santopinto, arXiv:1911.00960.
- [38] Z.-G. Wang, *Eur. Phys. J. C* **77**, 432 (2017).
- [39] W. Chen, H.-X. Chen, X. Liu, T. G. Steele, and S.-L. Zhu, *Phys. Lett. B* **773**, 247 (2017).
- [40] Y. Bai, S. Lu, and J. Osborne, *Phys. Lett. B* **798**, 134930 (2019).
- [41] W. Heupel, G. Eichmann, and C. S. Fischer, *Phys. Lett. B* **718**, 545 (2012).
- [42] V. R. Debastiani and F. S. Navarra, *Chin. Phys. C* **43**, 013105 (2019).
- [43] A. V. Berezhnoy, A. K. Likhoded, A. V. Luchinsky, and A. A. Novoselov, *Phys. Rev. D* **84**, 094023 (2011).
- [44] M. Karliner, S. Nussinov, and J. L. Rosner, *Phys. Rev. D* **95**, 034011 (2017).
- [45] J.-M. Richard, A. Valcarce, and J. Vijande, *Phys. Rev. D* **95**, 054019 (2017).
- [46] J. Wu, Y.-R. Liu, K. Chen, X. Liu, and S.-L. Zhu, *Phys. Rev. D* **97**, 094015 (2018).
- [47] X. Chen, *Eur. Phys. J. A* **55**, 106 (2019).
- [48] M.-S. Liu, Q.-F. Lü, and X.-H. Zhong and Q. Zhao, *Phys. Rev. D* **100**, 016006 (2019).
- [49] G.-J. Wang, L. Meng, and S.-L. Zhu, *Phys. Rev. D* **100**, 096013 (2019).
- [50] J.-M. Richard, A. Valcarce, and J. Vijande, *Phys. Rev. C* **97**, 035211 (2018).
- [51] C. Hughes, E. Eichten, and C. T. H. Davies, *Phys. Rev. D* **97**, 054505 (2018).
- [52] E. J. Eichten and C. Quigg, *Phys. Rev. Lett.* **119**, 202002 (2017).
- [53] M. Karliner and J. L. Rosner, *Phys. Rev. Lett.* **119**, 202001 (2017).
- [54] E. Hernández, J. Vijande, A. Valcarce, and J.-M. Richard, *Phys. Lett. B* **800**, 135073 (2019).
- [55] C. E. Fontoura, G. Krein, A. Valcarce, and J. Vijande, *Phys. Rev. D* **99**, 094037 (2019).
- [56] J. Carlson, L. Heller, and J. A. Tjon, *Phys. Rev. D* **37**, 744 (1988).
- [57] D. Ebert, R. N. Faustov, V. O. Galkin, and W. Lucha, *Phys. Rev. D* **76**, 114015 (2007).
- [58] L. Leskovec, S. Meinel, M. Pflaumer, and M. Wagner, *Phys. Rev. D* **100**, 014503 (2019).
- [59] A. Francis, R. J. Hudspith, R. Lewis, and K. Maltman, *Phys. Rev. Lett.* **118**, 142001 (2017).
- [60] P. Junnarkar, N. Mathur, and M. Padmanath, *Phys. Rev. D* **99**, 034507 (2019).
- [61] S. S. Agaev, K. Azizi, and H. Sundu, arXiv:1905.07591.
- [62] A. Francis, R. J. Hudspith, R. Lewis, and K. Maltman, *Phys. Rev. D* **99**, 054505 (2019).
- [63] A. Ali, Q. Qin, and W. Wei, *Phys. Lett. B* **785**, 605 (2018).
- [64] A. Ali, A. Ya. Parkhomenko, Q. Qin, and W. Wang, *Phys. Lett. B* **782**, 412 (2018).
- [65] G. K. C. Cheung, C. E. Thomas, J. J. Dudek, and R. G. Edwards, *J. High Energy Phys.* **11** (2017) 033.
- [66] S. S. Agaev, K. Azizi, and H. Sundu, *Phys. Rev. D* **99**, 114016 (2019).
- [67] Y. Yang and J. Ping, *Phys. Rev. D* **99**, 094032 (2019).
- [68] Z.-G. Wang, *Eur. Phys. Lett.* **128**, 11001 (2019).
- [69] E. Hiyama, Y. Kino, and M. Kamimura, *Prog. Part. Nucl. Phys.* **51**, 223 (2003).
- [70] A. Valcarce, F. Fernández, P. Gonzalez, and V. Vento, *Phys. Lett. B* **367**, 35 (1996).
- [71] J. Segovia, D. R. Entem, and F. Fernandez, *Phys. Lett. B* **662**, 33 (2008).
- [72] J. Segovia, A. M. Yasser, D. R. Entem, and F. Fernández, *Phys. Rev. D* **78**, 114033 (2008).
- [73] P. G. Ortega, J. Segovia, D. R. Entem, and F. Fernández, *Phys. Rev. D* **94**, 114018 (2016).
- [74] G. Yang, J. Ping, and J. Segovia, *Few-Body Syst.* **59**, 113 (2018).
- [75] G. Yang, J. Ping, P. G. Ortega, and J. Segovia, *Chin. Phys. C* **44**, 023102 (2020).
- [76] F. Fernandez, A. Valcarce, U. Straub, and A. Faessler, *J. Phys. G* **19**, 2013 (1993).
- [77] A. Valcarce, A. Buchmann, F. Fernández, and A. Faessler, *Phys. Rev. C* **50**, 2246 (1994).
- [78] P. G. Ortega, J. Segovia, D. R. Entem, and F. Fernández, *Phys. Rev. D* **81**, 054023 (2010).
- [79] P. G. Ortega, J. Segovia, D. R. Entem, and F. Fernández, *Phys. Rev. D* **94**, 074037 (2016).
- [80] P. G. Ortega, J. Segovia, D. R. Entem, and F. Fernández, *Phys. Rev. D* **95**, 034010 (2017).
- [81] J. Vijande, A. Valcarce, and K. Tsushima, *Phys. Rev. D* **74**, 054018 (2006).
- [82] G. Yang, J. Ping, and F. Wang, *Phys. Rev. D* **95**, 014010 (2017).
- [83] G. Yang and J. Ping, *Phys. Rev. D* **97**, 034023 (2018).
- [84] G. Yang, J. Ping, and J. Segovia, *Phys. Rev. D* **99**, 014035 (2019).
- [85] S. Aoyama, T. Myo, K. Kato, and K. Ikeda, *Prog. Theor. Phys.* **116**, 1 (2006).
- [86] T. Myo, Y. Kikuchi, H. Masui, and K. Kato, *Prog. Part. Nucl. Phys.* **79**, 1 (2014).
- [87] M. Oka, S. Maeda, and Y.-R. Liu, *Intl. J. Mod. Phys.* **49**, 1960004 (2019).
- [88] J. Aguilar and J. M. Combes, *Commun. Math. Phys.* **22**, 269 (1971).
- [89] E. Balslev and J. M. Combes, *Commun. Math. Phys.* **22**, 280 (1971).
- [90] G. S. Bali, H. Neff, T. Düssel, T. Lippert, and K. Schilling, *Phys. Rev. D* **71**, 114513 (2005).
- [91] M. D. Scadron, *Phys. Rev. D* **26**, 239 (1982).
- [92] M. Harvey, *Nucl. Phys.* **A352**, 326 (1981).
- [93] J. Vijande, A. Valcarce, and N. Barnea, *Phys. Rev. D* **79**, 074010 (2009).
- [94] T. F. Caramés, J. Vijande, and A. Valcarce, *Phys. Rev. D* **99**, 014006 (2019).